Research article

Rogelio O. Caballero-Pérez*, Julián Bravo-Castillero and Leslie D. Pérez-Fernández

A simple scheme for calculating the energy harvesting figures of merit of porous ceramics

https://doi.org/10.1515/ehs-2021-0001
Received February 18, 2021; accepted February 28, 2021;
published online March 25, 2021

Abstract: We propose a scheme based on recursively applying analytical formulae for effective properties to a class of porous ceramics for calculating their energy harvesting figures of merit. We approximate the structure of freeze-cast PZT parallel laminae joined by links (or bridges) by a model that can be broken down into two directions along which the structure resembles a laminate. The effective coefficients obtained in the first step of the recursion are then used as input on the second step which gives the final effective moduli. The comparison of those with calculations via Finite Element Method (FEM) on a non-recursive model shows good agreement. Finally, we calculate the piezoelectric and pyroelectric figures of merit and compare them with experimental results. The proposed scheme is a good alternative since it relies only on known simple analytical formulae and has a very low computational cost with respect to other methods that may be applied to such a geometry.

Keywords: figures of merit; homogenization; piezoelectricity; porous ceramics; pyroelectricity.

***Corresponding author: Rogelio O. Caballero-Pérez**, Instituto de Investigaciones en Matemáticas Aplicadas y en Sistemas, Universidad Nacional Autónoma de México, Unidad Académica del IIMAS en el Estado de Yucatán, Parque Científico y Tecnológico de Yucatán, CP 97302, Mérida, Yucatán, Mexico,
E-mail: rogelio.caballero@iimas.unam.mx. https://orcid.org/0000-0002-5474-174X
Julián Bravo-Castillero, Instituto de Investigaciones en Matemáticas Aplicadas y en Sistemas, Universidad Nacional Autónoma de México, Unidad Académica del IIMAS en el Estado de Yucatán, Parque Científico y Tecnológico de Yucatán, CP 97302, Mérida, Yucatán, Mexico, E-mail: julian@mym.iimas.unam.mx
Leslie D. Pérez-Fernández, Departamento de Matemática e Estatística, Instituto de Física e Matemática, Universidade Federal de Pelotas, Caixa Postal 354, CEP 96010-900, Pelotas, Rio Grande do Sul, Brazil, E-mail: leslie.fernandez@ufpel.edu.br

Introduction

The most intuitive and natural magnitudes for quantifying the piezoelectric and pyroelectric energy-harvesting capabilities of materials are the electro-mechanical and electro-thermal coupling factors as they represent the ratios of transformation of one form of input energy to other form of stored energy (Berlincourt, Curran, and Jaffe 1964; Bowen et al. 2015). However, these coupling coefficients rule out certain materials due to their relatively low compliances. In order to solve this problem, the following Figures of Merit have been proposed as better measures (Bowen et al. 2015; Deutz et al. 2018):

$$\mathrm{FoM}_{3j} = \frac{\widehat{d}_{3j}^{2}}{\widehat{\kappa}_{33}^{T}}, \quad F_E' = \frac{\left(\widehat{p}^{T}\right)^{2}}{\widehat{\kappa}_{33}^{T}\widehat{C}_E^{2}}. \tag{1}$$

where $\widehat{d}_{3j}$, j = 1, 2, 3 and $\widehat{\kappa}_{33}^{T}$ are the piezoelectric and dielectric coefficients at constant stress. $\widehat{C}_E$ represents the volume specific heat capacity. The subscript 3 represents the direction of polarization of the transversely isotropic ceramic.

Recently, in (Zhang et al. 2017), it was shown that ceramics with highly aligned porosity, manufactured via freeze-casting, have improved energy-harvesting FoMs (1) with respect to their dense (non-porous) counterparts made of the same material. This effect is due to the steeper reduction of the dielectric permittivity and heat capacity with respect to the reduction of the piezoelectric and pyroelectric coefficients as porosity increases.

From a modeling standpoint, the experimental samples obtained via the technique described in (Zhang et al. 2017), may be considered as ceramic-air composites that approximately exhibit 2-2 connectivity, where the first number indicates the connectivity of the ceramic and the second number the connectivity of the pore regions (Newnham, Skinner, and Cross 1978). The laminated 2-2 structure is interesting for its simplicity, mechanical strength (Zhang et al. 2017) and enhanced sensing and actuation capabilities (Roscow et al. 2015).

The measurements of (Zhang et al. 2017) were successfully fitted to phenomenological models based on

the rule of mixtures that compute the effective coefficients involved in (1). However, it would be desirable to have a model from first prinicples that is also easy to implement. The high alignment of the pores and their periodic distribution suggest the use of the mathematical homogenization, for computing its effective thermo-piezoelectric coefficients and, ultimately, their FoMs. In the case of a 2-2 connected composite, there exist analytical formulae for the effective coefficients (Caballero-Pérez et al. 2019; Sixto-Camacho et al. 2013). However, the specimens from (Zhang et al. 2017) exhibit ceramicbridges between contiguous laminae that break the perfect 2-2 connectivity. These bridges are indeed an important feature since they provide high compressive strength to the sample and disrupt the complete polarization of the ceramic occupied regions.

In order to account for the bridges, we present a two-step Recursive Homogenization Scheme (RHS). The RHS has been used to compute the elastic effective properties of 3-1 connected, non-porous composites with coating on the fibers (Guinovart-Díaz et al. 2005). This application was successfully compared with calculations based on a self-consistent Mori-Tanaka scheme for a 3-phases, fiber-reinforced composite. The piezoelectric and dielectric properties have also been calculated via RHS for a 3-1 connected composite with rectangle-shaped cross section of the fibers (Otero et al. 2003). These results showed good agreement with experimental measurements of quantities that are relevant for ultrasound applications. In (Brenner, Bravo-Castillero, and Mesejo-León 2012), the RHS was used to compute the effective electro-mechanical properties of two-phase fibrous-laminate, non-porous structure. These results were validated with a homogenization method based on the Fast Fourier Transform algorithm.

In this work we use a RHS that consists of two steps. In the first one, the bridges are homogenized using formulae for ceramic-air composites. The resulting partial effective elastic, piezoelectric, dielectric and pyroelectric coefficients are fed as input to the formulae that is used in the second step to obtain the final effective coefficients and homogenize the composite. In the particular case of the present structure, the RHS may be broken down into computing the effective coefficients of two laminates, which is convenient since homogenization gives analytical formulae for 2-2 composites (Bravo-Castillero et al. 2009). Hence, the calculations are a straight-forward process with minimal computational requirements as there is no need to create any geometry-specific meshes or to solve any systems of equations. All of the effective coefficients that are relevant to piezoelectric and pyroelectric FoMs can be obtained through RHS.

In the next section we present the geometrical model of the structure and the steps of the recursion. For each step, the analytical formulae for the effective coefficients of laminates and are stated. In the Results section, the RHS is compared to FEM calculations of the effective properties.

Methodology

The mathematical model represents a *non-ideal* 2-2 connected ceramic with pores. We say that the 2-2 connectivity is non-ideal because consecutive laminae are connected by small bridges. These defects are the result of the freeze-casting method that was used to synthetize the experimental samples, as can be seen on Figure 2 of (Zhang et al. 2017). The mathematical model of this structure is shown in Figure 1. It is composed by parallel, periodically distributed laminae that are connected by another set of relatively thinner laminae. The spaces between ceramic-occupied regions are assumed to be void.

Roughly, the RHS consists in recursively homogenizing along two directions that are shown with gray arrows in Figure 1. In the first step, we homogenize a laminate that extends vertically and it is composed by the bridges and the air gaps between them. The effective coefficients derived from this homogenization process are then assigned to an imaginary phase that is homogenized along with the thicker laminae in the second step. Notice that in each one of the steps, 2-2 composites are homogenized, the only difference being that in the first step one of the phases has material properties equal to zero. There exist analytical formulae for both scenarios.

The coefficients (or moduli) that are relevant to the present scheme are: the elastic, c_{ij}; the piezoelectric, e_{ij}; the dielectric, κ_{ij}; the thermoelastic, λ_i and pyroelectric, p^{ε} and the volume specific heat capacity C_E. The superscript ε indicates properties at constant strain to differentiate them from those at constant stress with superscript T. In the next sections we will see how to obtain the effective coefficients that appear in the FoMs (1).

First step

In this step we are going to compute the effective coefficients of an air-ceramic laminate whose phases are the bridges between the larger laminae and the air gaps between them. This composite extends along the direction of x_1 (vertical gray arrow in the upper left of Figure 1). The volume of the periodic cell (lower panel Figure 1) is equal to one, the fraction of it that is occupied by the bridge is v_1, the volume occupied by air is v_2 and the volume occupied by the ceramic laminae is v_3, so $v_1 + v_2 + v_3 = 1$. Taking into account these volume fractions, we can determine the volume fraction of the pore θ relative to the composite that we are homogenizing on the first step:

$$\theta = \frac{v_2}{v_2 + v_1}$$

The formulae for the effective coefficients of these composites can be derived from those that can be found for laminates on (Caballero-Pérez et al. 2019; Sixto-Camacho et al. 2013) by taking the limit when the moduli of one of the components go to zero, so as to model the properties of air. In this step, all of them except for the formula for the heat capacity C_E, correspond exactly to the rule of mixtures:

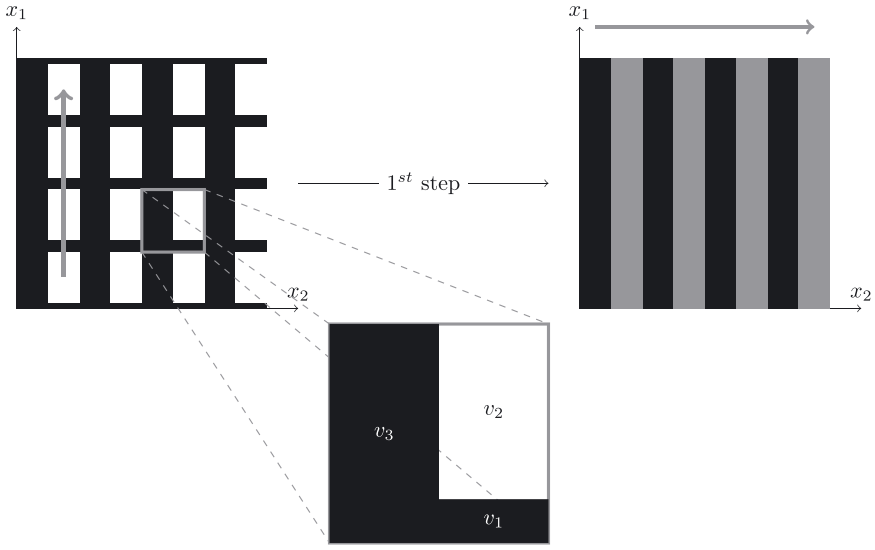

Figure 1: Representative cross section of the model (upper left) and a periodic cell (below). The regions occupied by ceramic are shown in black. The thickness of the ceramic bridges (horizontal stripes) is exaggerated for clarity. The gray thick arrow indicates the direction of homogenization in the first step. In the upper right, the gray areas represent the homogeneous material that results from homogenizing the ceramic bridges-air composite, and the direction of homogenization in the second step. The x_3 axis is perpendicular to the plane of the figure.

$$\begin{aligned}
&\tilde{c}_{22} = c_{22}(1-\theta), \quad \tilde{c}_{33} = c_{33}(1-\theta), \quad \tilde{c}_{23} = c_{23}(1-\theta), \tilde{e}_{32} = e_{32}(1-\theta), \quad (2)\\
&\tilde{e}_{33} = e_{33}(1-\theta), \quad \tilde{\kappa}^{\epsilon}_{33} = \kappa^{\epsilon}_{22}(1-\theta), \quad \tilde{\lambda}_2 = \lambda_2(1-\theta), \quad \tilde{\lambda}_3 = \lambda_3(1-\theta),\\
&\tilde{p}^{\epsilon} = p^{\epsilon}(1-\theta), \quad \tilde{C}_E = (C_E - T_r\lambda_1^2 c_{11}^2)(1-\theta),
\end{aligned}$$

where T_r = 300 K represents a reference temperature and the tilde $\tilde{\cdot}$ indicates an effective property of the first step, which in the second step will be used as the property of one of the phases. All other effective properties are either equal to zero or do not appear in the formulae of the second step.

Second step

More effective coefficients are non-zero in this step due to the fact that we are homogenizing two phases, none of which is air, along the direction of the horizontal gray arrow in Figure 1. The effective moduli of the second step are the definitive ones for this particular model:

$$\begin{aligned}
&\widehat{c}_{11} = \langle c_{11}\rangle - \langle c_{12}^2 c_{22}^{-1}\rangle + \langle c_{12} c_{22}^{-1}\rangle^2 \langle c_{22}^{-1}\rangle^{-1}, \quad (3)\\
&\widehat{c}_{22} = \langle c_{22}^{-1}\rangle^{-1},\\
&\widehat{c}_{33} = \langle c_{33}\rangle - \langle c_{23}^2 c_{22}^{-1}\rangle + \langle c_{23} c_{22}^{-1}\rangle^2 \langle c_{22}^{-1}\rangle^{-1},\\
&\widehat{c}_{12} = \langle c_{12} c_{22}^{-1}\rangle \langle c_{22}^{-1}\rangle^{-1},\\
&\widehat{c}_{13} = \langle c_{13}\rangle - \langle c_{12} c_{23} c_{22}^{-1}\rangle + \langle c_{12} c_{22}^{-1}\rangle \langle c_{23} c_{22}^{-1}\rangle \langle c_{22}^{-1}\rangle^{-1},\\
&\widehat{c}_{23} = \langle c_{23} c_{22}^{-1}\rangle \langle c_{22}^{-1}\rangle^{-1},\\
&\widehat{e}_{31} = \langle e_{31}\rangle - \langle e_{31} c_{12} c_{22}^{-1}\rangle + \langle e_{32} c_{22}^{-1}\rangle \langle c_{12} c_{22}^{-1}\rangle \langle c_{22}^{-1}\rangle^{-1},\\
&\widehat{e}_{32} = \langle e_{32} c_{22}^{-1}\rangle \langle c_{22}^{-1}\rangle^{-1},\\
&\widehat{e}_{33} = \langle e_{33}\rangle + \langle c_{32} c_{22}^{-1}\rangle \langle e_{32} c_{22}^{-1}\rangle \langle c_{22}^{-1}\rangle)^{-1} - \langle c_{32} e_{32} c_{22}^{-1}\rangle,\\
&\widehat{\kappa}^{\epsilon}_{33} = \langle \kappa^{\epsilon}_{33}\rangle + \langle e_{32}^2 c_{22}^{-1}\rangle - \langle e_{32} c_{22}^{-1}\rangle^2 \langle c_{22}^{-1}\rangle^{-1},\\
&\widehat{\lambda}_1 = \langle \lambda_1\rangle + \langle c_{12} c_{22}^{-1}\rangle \langle c_{22}^{-1}\rangle^{-1} \langle c_{22}^{-1}\lambda_2\rangle - \langle c_{12} c_{22}^{-1}\lambda_2\rangle,\\
&\widehat{\lambda}_2 = \langle c_{22}^{-1}\rangle^{-1} \langle c_{22}^{-1}\lambda_2\rangle,\\
&\widehat{\lambda}_3 = \langle \lambda_3\rangle + \langle c_{32} c_{22}^{-1}\rangle \langle c_{22}^{-1}\rangle \langle c_{22}^{-1}\lambda_2\rangle - \langle c_{32} c_{22}^{-1}\lambda_2\rangle,\\
&\widehat{p}^{\epsilon} = \langle p^{\epsilon}\rangle - \langle e_{32} c_{22}^{-1}\rangle \langle c_{22}^{-1}\rangle^{-1} \langle \lambda_2 c_{22}^{-1}\rangle + \langle e_{32}\lambda_2 c_{22}^{-1}\rangle,\\
&\widehat{C}_E = \langle C_E\rangle + T_r \langle \lambda_2 c_{22}^{-1}\rangle^2 \langle c_{22}^{-1}\rangle^{-1} + T\langle \lambda_2^2 c_{22}^{-1}\rangle.
\end{aligned}$$

The brackets $\langle\cdot\rangle$ represent the average of the modulus between them weighted by the volume fractions. The hat $\widehat{\cdot}$ represents the effective properties of the second step that are a function of the properties of the material and the effective coefficients of the first step (2). For example, the extended formulae for $\widehat{c}_{22}$ and $\widehat{e}_{32}$ is:

$$\widehat{c}_{22} = \frac{1}{\frac{v_3}{c_{22}} + \frac{1-v_3}{\tilde{c}_{22}}}, \quad \widehat{e}_{32} = \frac{\frac{e_{32}}{c_{22}} v_3 + \frac{\tilde{e}_{32}}{\tilde{c}_{22}}(1-v_3)}{\frac{v_3}{c_{22}} + \frac{1-v_3}{\tilde{c}_{22}}}$$

These formulae discussed in this subsection are valid when the direction x_3 of the polarization of the transversely isotropic material is perpendicular to the direction of the periodicity x_2. This is known as parallel polarization. When the periodicity and polarization directions coincide, we say that the polarization is series. There exist analytical formulae for this case (Caballero-Pérez et al. 2019; Sixto-Camacho et al. 2013), but we will not show them for brevity.

Figures of merit

Once the definitive effective coefficient of the porous ceramic have been calculated we turn to the calculation of the FoMs. Observe that the coefficients that appear in expressions (1) are at constant stress while those obtained through homogenization are at constant strain. Hence, we need to transform them through the following expressions:

$$\begin{aligned}
\widehat{d}_{3j} &= \widehat{e}_{31}\widehat{s}_{1j} + \widehat{e}_{32}\widehat{s}_{2j} + \widehat{e}_{33}\widehat{s}_{3j}\\
\widehat{\kappa}^{T}_{33} &= \widehat{\kappa}^{\epsilon}_{33} + \sum_{l=1}^{3} \widehat{d}_{3l}\widehat{e}_{3l}\\
\widehat{p}^{T} &= \widehat{p}^{\epsilon} + \sum_{l=1}^{3}\sum_{j=1}^{3} \widehat{e}_{3l}\widehat{s}_{lj}\widehat{\lambda}_j\\
\widehat{\beta}^{T} &= \widehat{\beta}^{\epsilon} + T_r \sum_{l=1}^{3}\sum_{j=1}^{3} \widehat{\lambda}_l\widehat{s}_{lj}\widehat{\lambda}_j
\end{aligned}$$

where $\widehat{s}_{lj}$ are the components of the compliance tensor that may be found by inverting the stiffness tensor when it is expressed in Voigt's notation (see appendix of (Belytschko, Liu, and Moran 2000)). However, due to the form of these tensors for transversely isotropic symmetry (Berlincourt, Curran, and Jaffe 1964), we only need to invert the upper 3×3 diagonal block of the stiffness tensor to get the relevant compliance components:

$$\begin{pmatrix} \widehat{s}_{11} & \widehat{s}_{12} & \widehat{s}_{13} \\ \widehat{s}_{21} & \widehat{s}_{22} & \widehat{s}_{23} \\ \widehat{s}_{31} & \widehat{s}_{32} & \widehat{s}_{33} \end{pmatrix} = \begin{pmatrix} c_{11} & c_{12} & c_{13} \\ c_{21} & c_{22} & c_{23} \\ c_{31} & c_{32} & c_{33} \end{pmatrix}^{-1}$$

The inversion of the stiffnesses is what concentrates the best part of the computational cost of this method. This is an operation on a fixed size 3×3 matrix in contrast with FEM which would require operations on much larger matrices with sizes proportional to the number of nodes on the meshes. We fixed the bridge volume fraction at $\nu_1 = 0.1$ and calculated the effective properties and the figures of merit as functions of the pore volume fraction in an interval. These results are shown in the next section.

Results

In order to put the formulae to the test we are going to use the materials $BaTiO_3$ and PZT-51, whose moduli are shown on Table 1. The ceramic known as PZT-51 is the one that was used in the experiments of (Zhang et al. 2017). Since the manufacturer did not provide all of the required moduli, Dr. Zhang, one of the authors of (Zhang et al. 2017), pointed out that the material PCR-7 whose properties can be found on Table 1.5 of (Topolov, Bowen, and Bisegna 2018), is a good replacement.

In Figure 2, we show a comparison between these effective piezoelectric coefficients of porous $BaTiO_3$ computed via RHS and via FEM. The panels on the left column depict the parallel polarization while the right panels depict the same coefficients but in series polarization. As we can see there is a good agreement between both mathematical methods. The greatest deviations occur in the series polatization. This is due to the fact that the volume ν_1 occupied by bridges in the local cell is a free parameter that needs to be fitted. The influence of that parameter is greater in the series polarization. To explain that consider that when $\nu_1 \to 0$ there is no physical integrity along the direction of x_3 which causes singular behavior in some terms of formulae that contain harmonic means. However, the formulae for the parallel polarization work well for any volume of the bridges.

Table 1: Material data used in the formulae.

Property	$BaTiO_3$	PZT-51
c_{11} (GPa)	158	124.4
c_{12} (GPa)	69	83.4
c_{13} (GPa)	67.5	80.5
c_{33} (GPa)	150	120.2
e_{31} (C/m^2)	−3.1	5.6
e_{33} (C/m^2)	13.5	36.1
$\kappa_{33}^{\varepsilon}$ ($10^{-10} C^2/Nm^2$)	80.5	17.9
λ_1 (10^3 PaK^{-1})	4.3	4.3
λ_3 (10^3 PaK^{-1})	3.5	3.5
p (10^{-6} $Cm^{-2}K^{-1}$)	0	−7.6

In Figure 3 we show some components of the effective compliance tensor that are used in the calculation of $\widehat{d}_{3j}$. The left column comprises parallel effective coefficients while the right one, series effective coefficients. We can observe that overall there is good agreement between RHS and FEM. The result of multiplying these non-constant compliances shown on Figure 3 with the non constant piezoelectric coefficients shown on Figure 2 are the constant values $\widehat{d}_{31} = -0.05\, nC/N$ and $\widehat{d}_{33} = 0.14\, nC/N$ for the parallel polarization.

The piezoelectric FoMs FoM_{3j} are shown on Figure 4. There is an excellent agreement between both theoretical methods. The agreement with the experimental measurements is not optimal but it may be improved by taking into account the decrease in the overall polarization with increasing porosity due to the defects hampering the reorientation of the domains, as it is pointed out in (Zhang et al. 2017). The theoretical models do not account for this decrease since nowhere in literature it is experimentally quantified. Instead, for each polarization it is assumed that the piezoelectric coefficients e_{ij} for any region occupied by the ceramic are equal to those of the dense ceramic. The same difficulty occurs for the pyroelectric properties, something that is expected due to the relationship between them and piezoelectricity at the atomic level. Having the real pyroelectric property for each porosity would improve the match of the theoretical and experimental pyroelectric F_E' of expression $(1)_2$, as can be seen on Figure 5.

Discussion

The complex connectivity of the experimental samples can be simulated by a simple mathematical model whose effective properties we were able to calculate from first principles without the need of the empirical models that were used to explain the increase in the FoMs (Zhang et al. 2017). Homogenization yields analytical formulae for the effective coefficients that are used in both steps of the recursive scheme. This provides several advantages over numerical schemes as it reduces the computational costs and enables the analysis of the influence of certain material properties or moduli in the overall response of the porous ceramic. In this sense, the present approach represents a satisfactory compromise between mathematical rigour, ease of implementation and computational cost.

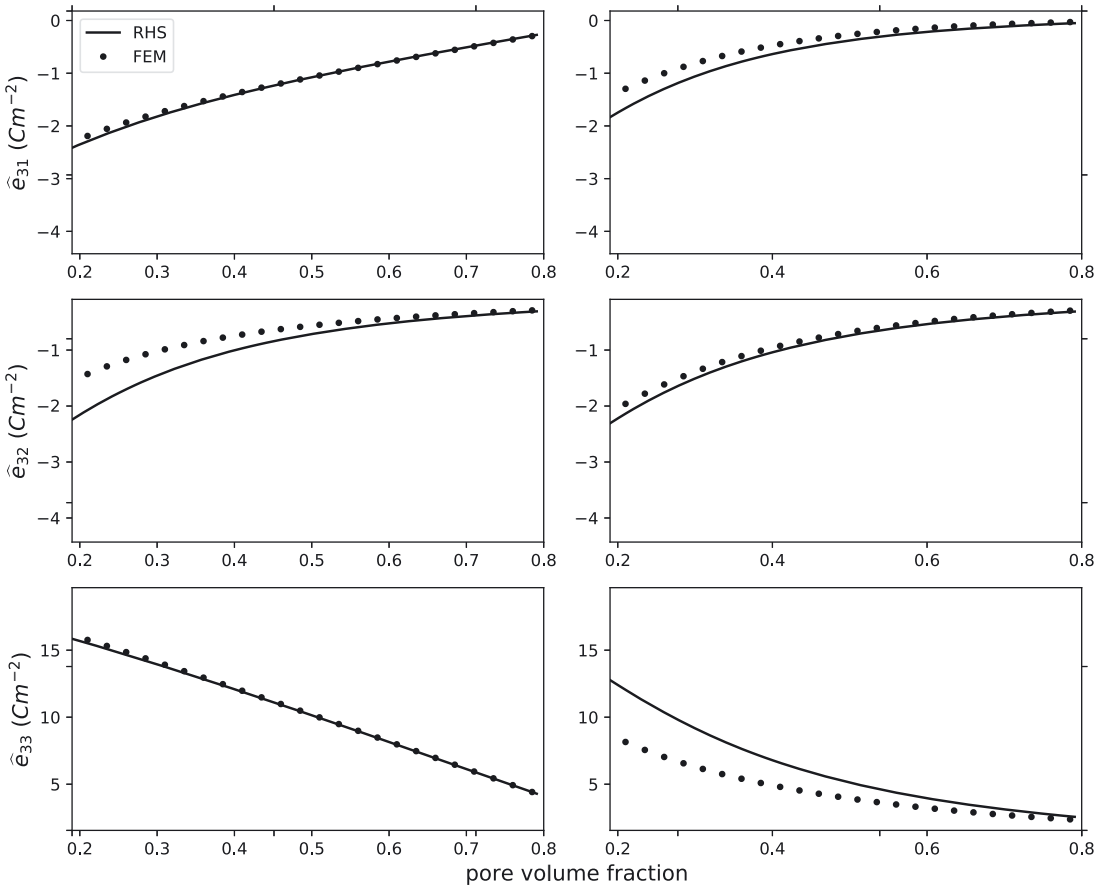

Figure 2: Effective components of the piezoelectric tensor at constant strain as functions of the pore volume fraction. Panels on the left (right) represent the parallel (series) polarization.

The piezoelectric and pyroelectric figures of merit obtained though RHS show good agreement with the experimental measurements, despite the fact that the present model does not take into account the lowered overall polarization associated to defects. In the case of series polarization, this feature is further accentuated due to the low interconnectivity of the ceramic in the direction of x_3. This effect is discussed in detail in (Zhang et al. 2017).

The RHS effective coefficients coincide with the results obtained by FEM. The advantage of RHS over FEM is evidenced in that the amount of time that it takes to calculate a full set of effective properties is negligible in comparison with FEM (tens of seconds in an Intel® Core ™ i5-3317U CPU @ 1.70 GHz × 4 processor). The agreement between theory and experiments may be further refined by considering the variation of properties with porosity due to a decrease in polarization as it is pointed out in (Zhang et al. 2017). This represents a way of fine-tuning the scheme for certain applications by considering properties for the bridges that are different to those of the larger laminae.

The RHS solely relies on the use of simple formulae (2) and (3) and it is flexible enough to account for different configurations of the polarization with respect to the pores. Furthermore, models of higher complexity can be treated via RHS just by adding additional steps to the recursion.

Additionally, another area in which this scheme may be significant is for predicting optimal properties for pyroelectric effects. Originally, the pyroelectric figures of merit that were proposed by Sebald, Lefeuvre, and Guyomar (2008), Sebald et al. (2006) involve coefficients in the Stress-Charge-Entropy, in contrast with the formula $(1)_2$ that has been used for the experimental studies. Coincidentally, the pyroelectric coefficient at constant strain $\widehat{p}_3^{\epsilon}$, exhibits an extremum which causes the simpler pyroelectric FoM:

$$F_E = \frac{\left(\widehat{p}^{\epsilon}\right)^2}{\widehat{\kappa}_{33}^{\epsilon}}$$

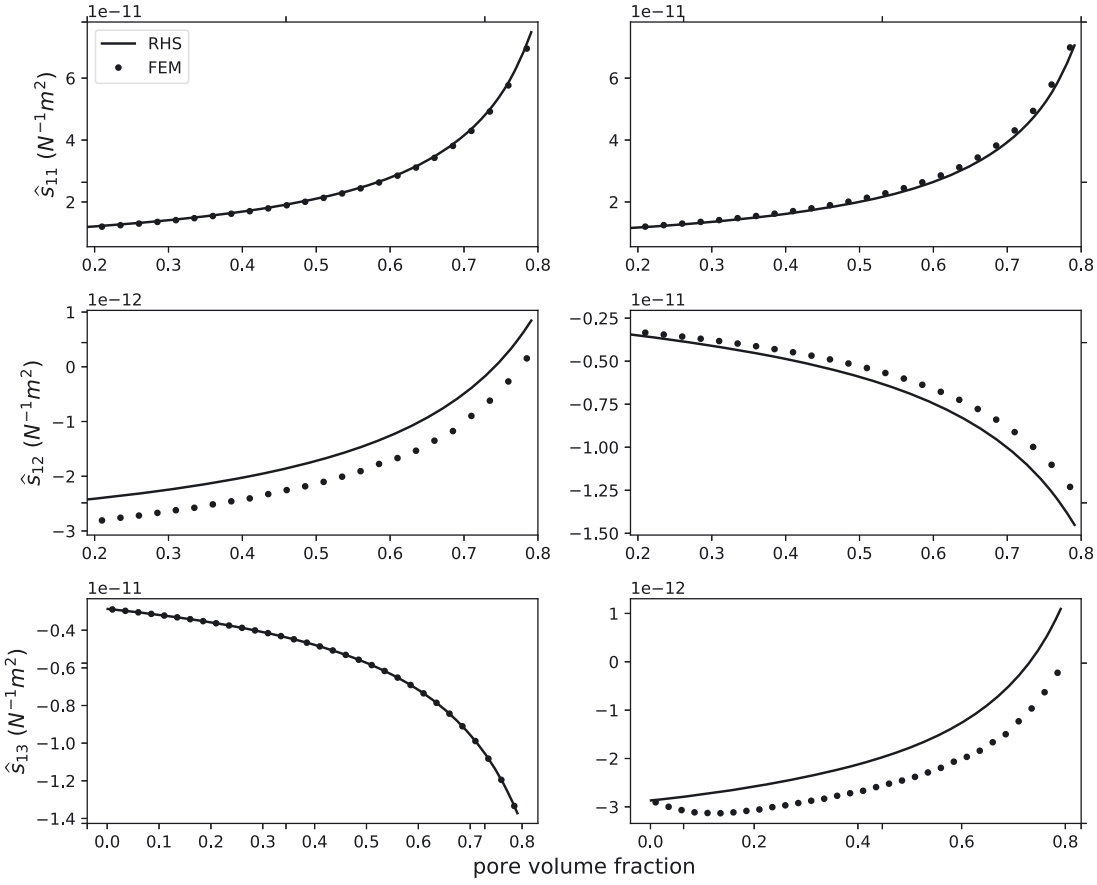

Figure 3: Effective components of the compliance tensor as functions of the pore volume fraction. Panels on the left (right) represent the parallel (series) polarization.

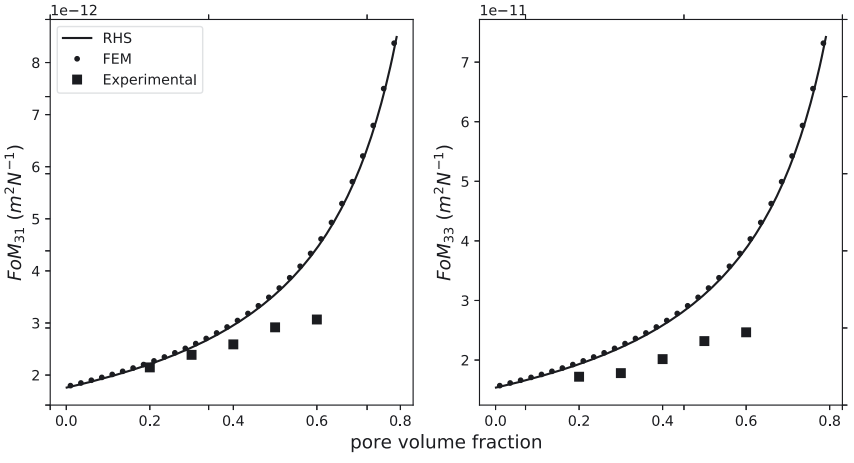

Figure 4: Piezoelectric figures of merit of porous PZT-51 computed via RHS vs experimental measurements of (Zhang et al. 2017).

to have a maximum. This figure of merit is shown on Figure 6. The maximum corresponds to optimal energy-harvesting capacity and the RHS may help to estimate the pore volume fraction in which the maximization occurs (in this case ≈0.044). This may help in avoiding trial and error approaches in design of devices. In this sense, the FoM $(1)_2$ does not provide useful information due to its strict monotonicity.

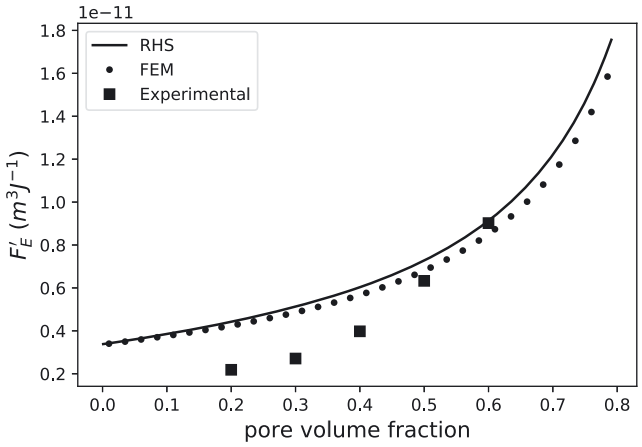

Figure 5: Pyroelectric figure of merit of PZT-51 computed via RHS vs experimental measurements of (Zhang et al. 2017).

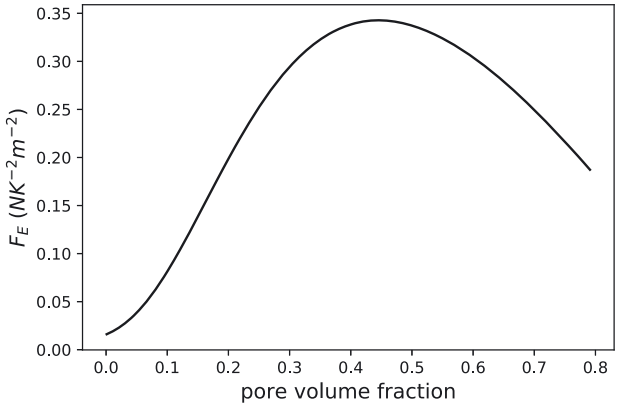

Figure 6: Pyroelectric figure of merit at constant strain computed via FEM and via RHS.

Acknowledgment: The authors are thankful to Yan Zhang PhD. for providing the experimental data and Ana Pérez Arteaga and Ramiro Chávez Tovar for technical assistance. The authors thank the hospitality of IIMAS-UNAM (Mérida Campus) during their research visit.

Author contributions: All the authors have accepted responsibility for the entire content of this submitted manuscript and approved submission.

Research funding: Financial support to this work was granted by the project PAPIIT-DGAPA-UNAM IA100919 and CONACyT (ROC's Ph.D. scholarship).

Conflict of interest statement: The authors declare no conflicts of interest regarding this article.

References

Belytschko, T., W. K. Liu, and B. Moran. 2000. *Nonlinear Finite Elements for Continua and Structures*. Chichester: John Wiley & Sons.

Berlincourt, D. A., D. R. Curran, and H. Jaffe. 1964. "Piezoelectric and Piezomagnetical Materials and Their Function in Transducers." In *Physical Acoustics*, 169–270. New York: Academic Press.

Bowen, C. R., J. Taylor, E. Le Boulbar, D. Zabeka, and V. Yu. Topolov. 2015. "A Modified Figure of Merit for Pyroelectric Energy Harvesting." *Journal of Mathematical Analysis and Applications* 138: 243–6.

Brenner, R., J. Bravo-Castillero, and D. Mesejo-León. 2012. "Investigation of the Effective Response of 2-1-2 Piezoelectric Composites." *Procedia IUTAM* 3: 292–300.

Bravo-Castillero, J., R. Rodríguez-Ramos, H. Mechkour, J. A. Otero, Y. Hernández-Cabanas, L. M. Sixto, R. Guinovart-Díaz, and F. J. Sabina. 2009. "Homogenization and Effective Properties of Periodic Thermomagnetoelectroelastic Composites." *Journal of Mechanics of Materials and Structures* 4: 819–36.

Caballero-Pérez, R. O., J. Bravo-Castillero, L. D. Pérez-Fernández, R. Rodríguez-Ramos, and F. J. Sabina. 2019. "Homogenization of Thermo-Magneto-Electro-Elastic Multilaminated Composites with Imperfect Contact." *Mechanics Research Communications* 97: 16–21.

Deutz, D. B., J. A. Pascoe, B. Schelen, S. van der Zwaag, D. M. de Leeuwa, and P. Groen. 2018. "Analysis and Experimental Validation of the Figure of Merit for Piezoelectric Energy Harvesters." *Materials Horizons* 5: 444–53.

Guinovart-Díaz, R., R. Rodríguez-Ramos, J. Bravo-Castillero, F. J. Sabina, J. A. Otero-Hernández, and G. A. Maugin. 2005. "A Recursive Asymptotic Homogenization Scheme for Multi-phase Fibrous Elastic Composites." *Mechanics of Materials* 37: 1119–31.

Newnham, R. E., D. P. Skinner, and L. E. Cross. 1978. "Connectivity and Piezoelectric-Pyroelectric Composites." *Materials Research Bulletin* 13: 525–36.

Otero, J. A., J. Bravo-Castillero, R. Guinovart-Díaz, R. Rodríguez-Ramos, and G. A. Maugin. 2003. "Analytical Expressions of Effective Constants for a Piezoelectric Composite Reinforced with Square Cross-Section Fibers." *Archives of Mechanics* 55: 357–71.

Roscow, J., Y. Zhang, J. Taylor, and C. R. Bowen. 2015. "Porous Ferroelectrics for Energy Harvesting Applications." *EPJ ST* 224: 2949–66.

Sebald, G., L. Seveyrat, D. Guyomar, L. Lebrun, B. Guiffard, and S. Pruvost. 2006. "Electrocaloric and Pyroelectric Properties of 0.75Pb(Mg1/3Nb2/3)O3 – 0.25PbTiO3 Single Crystals." *Journal of Applied Physics* 100: 124112.

Sebald, G., E. Lefeuvre, and D. Guyomar. 2008. "Pyroelectric Energy Conversion: Optimization Principles." *IEEE Transactions on Ultrasonics, Ferroelectrics, and Frequency Control* 55: 538–51.

Sixto-Camacho, L. M., J. Bravo-Castillero, R. Brenner, R. Guinovart-Díaz, H. Mechkour, R. Rodríguez-Ramos, and F. J. Sabina. 2013. "Asymptotic Homogenization of Periodic Thermo-Magneto-Electro-Elastic Heterogeneous Media." *Computers & Mathematics with Applications* 66: 2056–74.

Topolov, V. Y., C. R. Bowen, and P. Bisegna. 2018. "Piezo-Active Composites. Microgeometry-Sensitivity Relations." In *Springer Series in Materials Science 271*. Switzerland: Springer International Publishing.

Zhang, Y., M. Xie, J. Roscow, Y. Bao, K. Zhou, D. Zhang, and C. R. Bowen. 2017. "Enhanced Pyroelectric and Piezoelectric Properties of PZT with Aligned Porosity for Energy Harvesting Applications." *Journal of Materials Chemistry* 5: 6569–80.